Stability-constrained Optimal Power Flow for AC Microgrids with Convex Relaxation

Deepak Pullaguram, *Member, IEEE,* Ramtin Madani, *Member, IEEE,* and Ali Davoudi, *Senior Member, IEEE*

***Abstract*—This paper details and solves a stability-constrained optimal power flow (SCOPF) for inverter-based AC microgrids. To ensure sufficient stability margin during optimal generation, a small-signal stability constraint is embedded into the conventional OPF. This constraint is developed by satisfying a Lyapunov stability condition. A reduced-order model of the microgrid is adopted to alleviate the computational burden involved in solving the resulting SCOPF. Further, to tackle the non-convexity in SCOPF due to the presence of nonlinear power flow equations and stability constraint, two distinct convex relaxation approaches, namely semi-definite programming and parabolic relaxations, are developed. A penalty function is added to the objective function of the relaxed SCOPF, which is, then, solved sequentially to obtain a globally optimal solution. The efficacy of the proposed SCOPF is evaluated by performing numerical studies on multiple benchmarks as well as real-time studies on a 4-bus microgrid system built in a hardware-in-the-loop setup.**

***Index Terms*—AC Microgrids, Convex optimization, Optimal power flow, Relaxation, Stability.**

I. Introduction

MAJORITY of distributed generation units are interfaced with AC microgrids using inverters. Droop mechanism is a well-established decentralized control tool for proportional power sharing among inverters. This control approach alone does not ensure optimal operation or respect operational requirements usually dictated by the optimal power flows (OPFs) paradigms. An OPF-based droop adjustment is given in [1]. Varying droop parameters could cause small-signal stability issues [2], [3]. This paper details a OPF paradigm with improved small-signal stability margin that satisfies generation limits, power flow limits, and voltage constraints.

To enhance the stability margin, supplementary control loops [4], auxiliary stabilizers [5], [6], L_1-adaptive droop control [7], virtual droop frameworks [8], and lead compensators [9], are given as remedies. All these control methods are tuned for a selected range of operating points. Alternatively, the stability margin can be preventively improved by a proper generation dispatch. A stability-constrained optimal power flow (SCOPF) with stability constraints formulated based on state matrix sensitivities with respect to OPF variables is detailed in [10], [11]. The stability constraint is presented as a semi-definite programming (SDP) problem in [12], and the resulting SCOPF is transformed to a nonlinear optimization problem and solved using the interior-point method. SCOPF might lead to infeasible solutions due to its non-convex nature and the rigid threshold limits of the stability constraint [12]–[14]. To obtain a feasible solution, sequential quadratic programming and sequential optimization techniques, based on eigenvalue sensitivity matrix, are presented in [13] and [14], respectively. These dispatching schemes are developed for conventional power systems with synchronous generators, and rely on interior-point methods that are sensitive to initial conditions. The SCOPF of synchronous generator-based power systems in [15] uses the SDP relaxation technique to convexify the stability constraint based on a bilinear matrix inequality (BMI). This relaxation approach could potentially become computationally inefficient with the increase in number of generators and size of the power system.

Proper handling of the stability constraint is critical to the optimal-stable-feasible solution of the SCOPF problem in inverter-based microgrids. This paper illustrates the bilinear-matrix inequality (BMI) stability constraint derived from the Lyapunov stability condition. This constraint ensures sufficient stability margin by forcing the system spectral abscissa above a certain threshold. Since droop-controlled microgrids have myriad states [2], stability assessment considering detailed models will be computationally expensive. Alternatively, we adopt a reduced-order model [16] that incorporates only the dominant dynamics. Moreover, the BMI SCOPF is typically a non-convex and NP-hard problem due to nonlinear power, voltage, and stability constraints. To resolve this, nonlinear constraints are linearized by lifting SCOPF problem using auxiliary variables, and applying convex relaxations to resulting formulation. The optimal solution of the relaxed problem may not guarantee the feasibility with the original problem. A linear penalty function is added to the objective function of the relaxed problem, which is then solved sequentially until the optimal solution is obtained. The key contributions of the paper can be summarized as follows:

- SCOPF formulation for inverter-populated microgrids,
- convexifying the non-convex SCOPF using two relaxation approaches,
- achieving the globally optimal and feasible solution using sequential penalization.

The remainder of the paper has the following organization: Section II details notations used throughout the paper. The SCOPF problem is formulated in Section III. Section IV presents lifting, relaxation, and penalization of SCOPF to obtain a globally optimal solution. Numerical and experimental validations are given in Section V. Finally, Section VI concludes the paper.

D. Pullaguram was with the University of Texas at Arlington, USA. He is now with the National Institute of Technology, Warangal, India. R. Madani and A. Davioudi are with the University of Texas at Arlington, USA. This research is funded, in part, by the Office of Naval Research under award N00014-18-1-2186.

II. Notations

The italic lower case (a), bold-italic lower case ($\boldsymbol{a}$), and bold-italic upper case ($\boldsymbol{A}$) indicate scalars, vectors, and matrices, respectively. $\mathbb{R}$, $\mathbb{C}$, $\mathbb{S}^n$, and $\mathbb{H}^n$ represent sets of real numbers, complex numbers, $n \times n$ symmetric matrices, and hermitian matrices, respectively. The diagonal matrix with the '$\boldsymbol{a}$' vector of diagonal terms is shown by $[\boldsymbol{a}]$. $[\boldsymbol{a}]^n$ indicates the matrix formed by repeating the vector $\boldsymbol{a}$ for n columns. $(\cdot)^\top$ and $(\cdot)^*$ indicate the transpose and conjugate transpose of a matrix, respectively. $\mathbf{I}^n$ and 0^n indicate identity and zero matrices of size $n \times n$, respectively. The diagonal elements vector of a square matrix is shown by $\mathrm{diag}\{\cdot\}$. The absolute value of a vector or a scalar is given by $|\cdot|$. The trace of a matrix is shown by $\mathrm{tr}\{\cdot\}$. The frobenius norm of a matrix or a vector is represented by $\|\cdot\|$. The real and imaginary parts of the complex numbers are denoted by $\mathrm{Re}\{\cdot\}$ and $\mathrm{Im}\{\cdot\}$, respectively. The notation $\boldsymbol{a} \cdot \boldsymbol{b}$ indicates the element-wise product of vectors $\boldsymbol{a}$ and $\boldsymbol{b}$.

The AC microgrid has $\mathcal{N} = \{1, 2, ..., n\}$ set of buses on the power distribution network, $\mathcal{L} = \{1, 2, ..., l\} \subseteq \mathcal{N} \times \mathcal{N}$ set of distribution lines, and $\mathcal{G} = \{1, 2, ..., n^{\mathrm{g}}\}$ set of inverters. The vectors of the injected active and reactive powers are $\boldsymbol{p}^{\mathrm{g}} \in \mathbb{R}^{n^{\mathrm{g}} \times 1}$ and $\boldsymbol{q}^{\mathrm{g}} \in \mathbb{R}^{n^{\mathrm{g}} \times 1}$, respectively. An inverter incidence matrix, that locates inverters on the distribution bus, is defined as $\boldsymbol{G} \in \{0, 1\}^{n^{\mathrm{g}} \times n}$. The bus admittance matrix is given by $\boldsymbol{Y} \in \mathbb{C}^{n \times n}$. The $from$ and to admittance matrices are represented as $\vec{\boldsymbol{Y}}$, $\overleftarrow{\boldsymbol{Y}} \in \mathbb{C}^{n \times n}$, and their respective branch-incidence matrices as $\vec{\boldsymbol{L}}$, $\overleftarrow{\boldsymbol{L}} \in \{0, 1\}^{l \times n}$. Loads are considered as constant complex impedances, and included as shunt elements in $\boldsymbol{Y}$. $\boldsymbol{v}^{\mathrm{g}} \in \mathbb{C}^{n^{\mathrm{g}} \times 1}$ is the vector of bus voltages at point of coupling, and $\boldsymbol{v}^{\mathrm{b}} \in \mathbb{C}^{n - n^{\mathrm{g}} \times 1}$ is the vector of all remaining buses, such that $\boldsymbol{v} = \boldsymbol{v}^{\mathrm{g}} \bigcup \boldsymbol{v}^{\mathrm{b}}$. $\boldsymbol{v}^{\mathrm{o}}$ is the terminal voltages at inverter output terminals.

III. Stability-constrained Optimal Power Flow

A. OPF in AC Microgrids

The OPF for an AC microgrid is formulated as

$$
\begin{aligned}
\text{minimize} \quad & \mathrm{h}(\boldsymbol{p}^{\mathrm{g}}) && \text{(1a)}\\
\text{subject to} \quad & \boldsymbol{G}^\top(\boldsymbol{p}^{\mathrm{g}} + \mathrm{j}\boldsymbol{q}^{\mathrm{g}}) = \boldsymbol{d} + \mathrm{diag}\{\boldsymbol{v}\boldsymbol{v}^*\boldsymbol{Y}^*\} && \text{(1b)}\\
& \mathrm{diag}\{\vec{\boldsymbol{L}}\, \boldsymbol{v}\boldsymbol{v}^*\vec{\boldsymbol{Y}}^*\} \leq \boldsymbol{f}^{\max} && \text{(1c)}\\
& \mathrm{diag}\{\overleftarrow{\boldsymbol{L}}\, \boldsymbol{v}\boldsymbol{v}^*\overleftarrow{\boldsymbol{Y}}^*\} \leq \boldsymbol{f}^{\max} && \text{(1d)}\\
& \boldsymbol{p}^{\min} \leq \boldsymbol{p}^g \leq \boldsymbol{p}^{\max} && \text{(1e)}\\
& \boldsymbol{q}^{\min} \leq \boldsymbol{q}^g \leq \boldsymbol{q}^{\max} && \text{(1f)}\\
& (\boldsymbol{v}^{\min})^2 \leq |\boldsymbol{v}|^2 \leq (\boldsymbol{v}^{\max})^2 && \text{(1g)}\\
\text{varaibles} \quad & \boldsymbol{v} \in \mathbb{C}^{n \times 1}, \boldsymbol{p}^{\mathrm{g}} \in \mathbb{R}^{n^{\mathrm{g}} \times 1}, \boldsymbol{q}^{\mathrm{g}} \in \mathbb{R}^{n^{\mathrm{g}} \times 1}.
\end{aligned}
$$

$\mathrm{h}(\boldsymbol{p}^{\mathrm{g}})$ is assumed to be a quadratics cost function [17]

$$\mathrm{h}(\boldsymbol{p}^{\mathrm{g}}) = (\boldsymbol{p}^{\mathrm{g}})^\top [\boldsymbol{c}_2] \tilde{\boldsymbol{p}}^{\mathrm{g}} + \boldsymbol{c}_1^\top \boldsymbol{p}^{\mathrm{g}} + \boldsymbol{c}_0^\top \mathbf{1}^{n_{\mathrm{g}}}, \tag{2}$$

where c_2, c_1, and c_0 are the cost coefficients. The nodal power balance is enforced using (1b). The line flows are limited in either directions using (1c) and (1d). The active and reactive powers generated by individual inverters are bounded using (1e) and (1f), respectively. The constraint (1g) bounds the voltage magnitude within $[\boldsymbol{v}^{\min}, \boldsymbol{v}^{\max}]$. Next, additional constraints concerning system stability, inspired by the microgrid dynamics in [2], are needed to strengthen (1).

B. Incorporating Stability Constraint

To formulate the stability constraint, first, the microgrid is modeled as a set of differential-algebraic equations,

$$\dot{\boldsymbol{x}} = \boldsymbol{f}(\boldsymbol{x}, \boldsymbol{z}), \tag{3a}$$

$$0 = \boldsymbol{g}(\boldsymbol{x}, \boldsymbol{z}), \tag{3b}$$

where $\boldsymbol{f}$ and $\boldsymbol{g}$ represent the vectors of non-linear differential and algebraic equations of a microgrid, respectively. $\boldsymbol{x}$ and $\boldsymbol{z}$ are the vectors of state and algebraic variables of size n_{x} and n_{z}, respectively. To reduce the computational burden, a 3^{rd}-order inverter model [16] is adopted. The voltage and current controllers with LC filter in Fig. 1 have high closed-loop bandwidth compared to the power controller module, and one can safely assume that these control loops reach a quasi steady-state fast. Thus, the vector of differential equations, $\boldsymbol{f}$, with state variables $\boldsymbol{x} = [\boldsymbol{p}^\top, \boldsymbol{q}^\top, \boldsymbol{\delta}^\top]^\top \in \mathbb{R}^{n_{\mathrm{x}} \times 1}$, is composed of

$$\dot{\boldsymbol{p}} = -\boldsymbol{\omega}^c \cdot \boldsymbol{p} + \boldsymbol{\omega}^c \cdot \mathrm{Re}\{\boldsymbol{v}^{\mathrm{o}} \cdot (\boldsymbol{i}^{\mathrm{o}})^*\}, \tag{4a}$$

$$\dot{\boldsymbol{q}} = -\boldsymbol{\omega}^c \cdot \boldsymbol{q} + \boldsymbol{\omega}^c \cdot \mathrm{Im}\{\boldsymbol{v}^{\mathrm{o}} \cdot (\boldsymbol{i}^{\mathrm{o}})^*\}, \tag{4b}$$

$$\dot{\boldsymbol{\delta}} = (\boldsymbol{\omega} - \omega_{\mathrm{com}})\omega_{\mathrm{nom}}. \tag{4c}$$

Here, $\boldsymbol{\omega}_c \in \mathbb{R}^{n^{\mathrm{g}} \times 1}$ is the cutoff frequency of the low-pass filters used in power controller modules (Fig. 1). $\boldsymbol{p} \in \mathbb{R}^{n^{\mathrm{g}} \times 1}$ and $\boldsymbol{q} \in \mathbb{R}^{n^{\mathrm{g}} \times 1}$ are the filtered active and reactive power vectors, respectively. $\boldsymbol{v}^{\mathrm{o}} \in \mathbb{C}^{n^{\mathrm{g}} \times 1} = \boldsymbol{v}^{\mathrm{od}} + \mathrm{j}\boldsymbol{v}^{\mathrm{oq}}$ and $\boldsymbol{i}^{\mathrm{o}} \in \mathbb{C}^{n^{\mathrm{g}} \times 1} = \boldsymbol{i}^{\mathrm{od}} + \mathrm{j}\boldsymbol{i}^{\mathrm{oq}}$ are the inverter terminal's voltage and current, respectively. ω_{nom} and $\boldsymbol{\omega}$ are the microgrid nominal frequency and inverter operating frequency, respectively. $\boldsymbol{\delta}$ is the vector of inverter power angles with respect to a common reference, usually the inverter at bus 1 (i.e., $\omega_{\mathrm{com}} = \omega_1$). The operating frequency $\boldsymbol{\omega}$ is obtained using

$$\boldsymbol{\omega} \ = \omega_{\mathrm{nom}} - \boldsymbol{m}^p \cdot \boldsymbol{p} + \boldsymbol{m}^p \cdot \boldsymbol{p}^{\mathrm{opt}}, \tag{5}$$

where $\boldsymbol{p}^{\mathrm{opt}}$ is the active power set-point provided by the OPF, and $\boldsymbol{m}_p$ is the $p - \omega$ droop constant.

The vector of algebraic equations $\boldsymbol{g}$, with algebraic variables $\boldsymbol{z} = [(\boldsymbol{i}^{\mathrm{od}})^\top, (\boldsymbol{i}^{\mathrm{oq}})^\top]^\top \in \mathbb{R}_{\mathrm{z}}^n \times 1$, are given by

$$\boldsymbol{i}^{\mathrm{od}} = \mathrm{Re}\{\check{\boldsymbol{Y}}(\boldsymbol{v}^{\mathrm{o}} - \boldsymbol{i}^{\mathrm{o}} \cdot \boldsymbol{z}^{\mathrm{c}})\}, \tag{6a}$$

$$\boldsymbol{i}^{\mathrm{oq}} = \mathrm{Im}\{\check{\boldsymbol{Y}}(\boldsymbol{v}^{\mathrm{o}} - \boldsymbol{i}^{\mathrm{o}} \cdot \boldsymbol{z}^{\mathrm{c}})\}. \tag{6b}$$

$\check{\boldsymbol{Y}}$ is the Kron-reduced admittance matrix of the distribution network [16], $\boldsymbol{z}^{\mathrm{c}}$ is the impedance of the line connecting an inverter to the power distribution network, and

$$\boldsymbol{v}^{\mathrm{o}} = (\boldsymbol{v}^{\mathrm{opt}} + \boldsymbol{n}^q \cdot \boldsymbol{q}^{\mathrm{opt}} - \boldsymbol{n}^q \cdot \boldsymbol{q}) \cdot (\cos\boldsymbol{\delta} + \mathrm{j}\sin\boldsymbol{\delta}), \tag{7}$$

where $\boldsymbol{q}^{\mathrm{opt}}$ and $\boldsymbol{v}^{\mathrm{opt}}$ are the optimal reactive power and voltage set-points provided by the OPF, respectively. $\boldsymbol{n}_q$ is $q - v$ droop constant.

Proposition 1. *Consider a microgrid system defined by (3a) and (3b). Its small-signal stability, with a minimum decay rate*

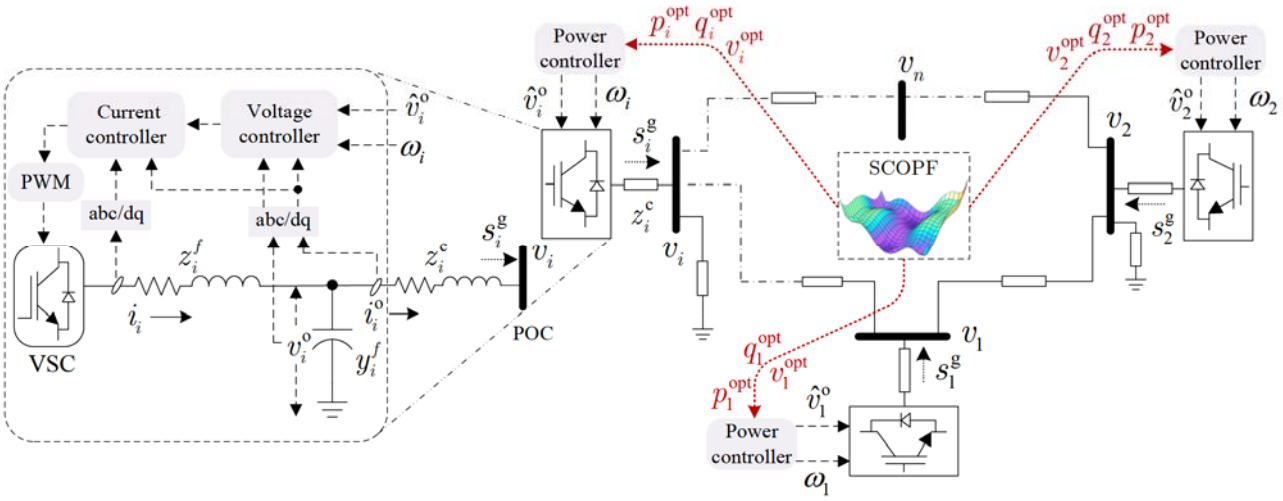

Fig. 1: AC microgrid schematic, inverter control, SCOPF optimization, and data flow

of η, can be assured [18] iff there exits a symmetric positive definite matrix $\boldsymbol{M}$ that satisfies

$$\hat{\boldsymbol{A}}^\top \boldsymbol{M} + \boldsymbol{M}\hat{\boldsymbol{A}} \preceq -2\eta \boldsymbol{M}, \tag{8}$$

where $\hat{\boldsymbol{A}}$ is the microgrid state matrix.

Proof. Linearizing (3a) and (3b) at the operating point $(\boldsymbol{x}_0, \boldsymbol{z}_0)$, using Taylor series expansion, gives

$$\begin{bmatrix} \Delta \dot{\boldsymbol{x}} \\ 0 \end{bmatrix} = \begin{bmatrix} \frac{\partial \boldsymbol{f}}{\partial \boldsymbol{x}} & \frac{\partial \boldsymbol{f}}{\partial \boldsymbol{z}} \\ \frac{\partial \boldsymbol{g}}{\partial \boldsymbol{x}} & \frac{\partial \boldsymbol{g}}{\partial \boldsymbol{z}} \end{bmatrix} \begin{bmatrix} \Delta \boldsymbol{x} \\ \Delta \boldsymbol{z} \end{bmatrix}. \tag{9}$$

The partial differential matrices $\frac{\partial \boldsymbol{f}}{\partial \boldsymbol{x}}$, $\frac{\partial \boldsymbol{f}}{\partial \boldsymbol{z}}$, $\frac{\partial \boldsymbol{g}}{\partial \boldsymbol{x}}$, and $\frac{\partial \boldsymbol{g}}{\partial \boldsymbol{z}}$ in (9) are given by (10)-(13), respectively. The $\boldsymbol{M}^{\mathrm{p}}$ in (10) is

$$\boldsymbol{M}^{\mathrm{p}} = \begin{bmatrix} -m_1^{\mathrm{p}} & m_2^{\mathrm{p}} & 0 & \cdots & 0 \\ -m_1^{\mathrm{p}} & 0 & m_3^{\mathrm{p}} & \cdots & 0 \\ \vdots & \vdots & \vdots & \ddots & 0 \\ -m_1^{\mathrm{p}} & 0 & 0 & \cdots & m_{n^g}^{\mathrm{p}} \end{bmatrix}, \tag{14}$$

where m_i^{p} indicates droop constant of i^{th} inverter. $\check{\boldsymbol{G}}$ and $\check{\boldsymbol{B}}$ are, respectively, the real and imaginary components of the Kron-reduced admittance matrix $\check{\boldsymbol{Y}}$.
Defining $\boldsymbol{A}(\boldsymbol{i}^{\mathrm{od}}, \boldsymbol{i}^{\mathrm{oq}}, \boldsymbol{\delta}, \boldsymbol{q}) = \frac{\partial \boldsymbol{f}}{\partial \boldsymbol{x}}$, $\boldsymbol{B}(\boldsymbol{\delta}, \boldsymbol{q}) = \frac{\partial \boldsymbol{f}}{\partial \boldsymbol{z}}$, $\boldsymbol{C}(\boldsymbol{\delta}, \boldsymbol{q}) = \frac{\partial \boldsymbol{g}}{\partial \boldsymbol{x}}$, and $\boldsymbol{D} = \frac{\partial \boldsymbol{g}}{\partial \boldsymbol{z}}$, and eliminating the algebraic variables $\boldsymbol{z}$, (9) can be reformulated [19] as,

$$\dot{\boldsymbol{x}} = \hat{\mathbf{A}}\boldsymbol{x}, \tag{15}$$

where $\hat{\boldsymbol{A}} \in \mathbb{R}^{n_{\mathrm{x}} \times n_{\mathrm{x}}}$ is the state matrix obtained by

$$\hat{\boldsymbol{A}} = \boldsymbol{A}(\boldsymbol{i}^{\mathrm{od}}, \boldsymbol{i}^{\mathrm{oq}}, \boldsymbol{\delta}, \boldsymbol{q}) - \boldsymbol{B}(\boldsymbol{\delta}, \boldsymbol{q})(\boldsymbol{D})^{-1}\boldsymbol{C}(\boldsymbol{\delta}, \boldsymbol{q}). \tag{16}$$

Consider a Lyapunov energy function, $V = \boldsymbol{x}^\top \boldsymbol{M}\boldsymbol{x}$, where $\boldsymbol{M} \in \mathbb{S}^{n_{\mathrm{x}}}$ is a symmetric positive definite matrix. Differentiating V, one has

$$\begin{aligned} \dot{V} &= \dot{\boldsymbol{x}}^\top \boldsymbol{M}\boldsymbol{x} + \boldsymbol{x}^\top \boldsymbol{M}\dot{\boldsymbol{x}}, \\ &= (\hat{\boldsymbol{A}}\boldsymbol{x})^\top \boldsymbol{M}\boldsymbol{x} + \boldsymbol{x}^\top \boldsymbol{M}\hat{\boldsymbol{A}}\boldsymbol{x}, \\ &= \boldsymbol{x}^\top (\hat{\boldsymbol{A}}^\top \boldsymbol{M} + \boldsymbol{M}\hat{\boldsymbol{A}})\boldsymbol{x}. \end{aligned} \tag{17}$$

For the microgrid to have a minimum damping (or decay rate) η, the necessary condition on the Lyapunov function [18] is

$$\dot{V} < -2\eta E. \tag{18}$$

From (17) and (18)

$$\hat{\boldsymbol{A}}^\top \boldsymbol{M} + \boldsymbol{M}\hat{\boldsymbol{A}} \preceq -2\eta \boldsymbol{M}, \tag{19a}$$

$$\boldsymbol{M} \succeq \mathrm{I}^{n_{\mathrm{x}}}. \tag{19b}$$

Proof of Proposition 1 is completed. □

To interlink the inverter internal variables with the OPF variables, additional constraints are formulated as

$$\boldsymbol{v}^{\mathrm{g}} = (\boldsymbol{v}^{\mathrm{ref}} - \boldsymbol{n}^q \cdot \boldsymbol{q}) \cdot (\cos\boldsymbol{\delta} + \mathrm{j}\sin\boldsymbol{\delta}) - \boldsymbol{i}^{\mathrm{o}} \cdot \boldsymbol{z}^c, \tag{20}$$

$$\boldsymbol{i}^{\mathrm{o}} = \check{\boldsymbol{Y}}\boldsymbol{v}^{\mathrm{g}}, \tag{21}$$

$$\boldsymbol{p} + \mathrm{i}\boldsymbol{q} = \mathrm{diag}\{\boldsymbol{i}^{\mathrm{o}}(\boldsymbol{i}^{\mathrm{o}})^*[\boldsymbol{z}^{\mathrm{c}}]\} + \boldsymbol{p}^g + \mathrm{i}\boldsymbol{q}^g, . \tag{22}$$

The OPF in (1), with additional constraints (19)-(22), constitute a SCOPF for an inverter-dominant microgrid. The constraints (1b)-(1g) are quadratic functions of the bus voltage $\boldsymbol{v}$. The state matrix $\hat{\boldsymbol{A}}$ in (19a), and the constraints (20) and (22), are non-linear functions of $\boldsymbol{i}^{\mathrm{o}}$, $\boldsymbol{q}$, and $\boldsymbol{\delta}$. These non-linearities make problem non-convex. In the next section, the SCOPF problem is lifted and relaxed to make it computationally tractable.

IV. Lifting, Relaxation, and Penalization

A. Lifted Formulation

The constraints (1b)-(1g) can be convexified by defining an auxiliary matrix $\boldsymbol{W} \in \mathbb{H}^n$ [20] as

$$\boldsymbol{W} \triangleq \boldsymbol{v}\boldsymbol{v}^*. \tag{23}$$

To convexify the constraints (20) and (22), and the state matrix $\hat{\boldsymbol{A}}$ in (19a), variables $\boldsymbol{\delta}^{\mathrm{c}} \in \mathbb{R}^{n_{\mathrm{g}} \times 1}$, $\boldsymbol{\delta}^{\mathrm{s}} \in \mathbb{R}^{n_{\mathrm{g}} \times 1}$, $\boldsymbol{\delta}^{\mathrm{qc}} \in \mathbb{R}^{n_{\mathrm{g}} \times 1}$, $\boldsymbol{\delta}^{\mathrm{qs}} \in \mathbb{R}^{n_{\mathrm{g}} \times 1}$, and a new vector, $\boldsymbol{u}_k \in \mathbb{R}^{n_u \times 1}\ \forall\ k \in \mathcal{G}$, are defined for each inverter as

$$\boldsymbol{\delta}^{\mathrm{c}} \triangleq \cos\boldsymbol{\delta}, \qquad \boldsymbol{\delta}^{\mathrm{s}} \triangleq \sin\boldsymbol{\delta}, \tag{24a}$$

$$\boldsymbol{\delta}^{\mathrm{qc}} \triangleq \boldsymbol{q} \cdot \cos\boldsymbol{\delta}, \quad \boldsymbol{\delta}^{\mathrm{qs}} \triangleq \boldsymbol{q} \cdot \sin\boldsymbol{\delta}, \tag{24b}$$

$$\boldsymbol{u}_k \triangleq [i_k^{\mathrm{od}}, i_k^{\mathrm{oq}}, \delta_k^{\mathrm{c}}, \delta_k^{\mathrm{s}}, q_k, \delta_k^{\mathrm{qc}}, \delta_k^{\mathrm{qs}}]^\top\ \forall k \in \mathcal{G}. \tag{24c}$$

$$\frac{\partial \mathbf{f}}{\partial \boldsymbol{x}} = \begin{bmatrix} -[\boldsymbol{\omega}^{\mathrm{c}}] & -\left[\boldsymbol{\omega}^{\mathrm{c}} \cdot \boldsymbol{n}^{q} \cdot (\boldsymbol{i}^{\mathrm{oq}} \cdot \sin\boldsymbol{\delta} + \boldsymbol{i}^{\mathrm{od}} \cdot \cos\boldsymbol{\delta})\right] & -\left[\boldsymbol{\omega}^{\mathrm{c}} \cdot (\boldsymbol{v}^{\mathrm{ref}} - \boldsymbol{n}^{q} \cdot \boldsymbol{q}) \cdot (\boldsymbol{i}^{\mathrm{od}} \cdot \sin\boldsymbol{\delta} - \boldsymbol{i}^{\mathrm{oq}} \cdot \cos\boldsymbol{\delta})\right] \\ 0^{n^{\mathrm{g}}} & \left[\boldsymbol{\omega}^{\mathrm{c}} \cdot \boldsymbol{n}^{\mathrm{q}} \cdot (\boldsymbol{i}^{\mathrm{oq}} \cdot \cos\boldsymbol{\delta} - \boldsymbol{i}^{\mathrm{od}} \cdot \sin\boldsymbol{\delta}) - \boldsymbol{\omega}^{\mathrm{c}}\right] & \left[\boldsymbol{\omega}^{\mathrm{c}} \cdot (\boldsymbol{v}^{\mathrm{ref}} - \boldsymbol{n}^{\mathrm{q}} \cdot \boldsymbol{q}) \cdot (\boldsymbol{i}^{\mathrm{od}} \cdot \cos\boldsymbol{\delta} + \boldsymbol{i}^{\mathrm{oq}} \cdot \sin\boldsymbol{\delta})\right] \\ \boldsymbol{M}^{\mathrm{p}} & 0^{n^{\mathrm{g}}-1} & 0^{n^{\mathrm{g}}-1} \end{bmatrix} \tag{10}$$

$$\frac{\partial \mathbf{f}}{\partial \boldsymbol{z}} = \begin{bmatrix} \left[\boldsymbol{\omega}^{\mathrm{c}} \cdot (\boldsymbol{v}^{\mathrm{ref}} - \boldsymbol{n}^{\mathrm{q}} \cdot \boldsymbol{q}) \cdot \cos\boldsymbol{\delta}\right] & \left[\boldsymbol{\omega}^{\mathrm{c}} \cdot (\boldsymbol{v}^{\mathrm{ref}} - \boldsymbol{n}^{\mathrm{q}} \cdot \boldsymbol{q}) \cdot \sin\boldsymbol{\delta}\right] \\ \left[\boldsymbol{\omega}^{\mathrm{c}} \cdot (\boldsymbol{v}^{\mathrm{ref}} - \boldsymbol{n}^{\mathrm{q}} \cdot \boldsymbol{q}) \cdot \sin\boldsymbol{\delta}\right] & -\left[\boldsymbol{\omega}^{\mathrm{c}} \cdot (\boldsymbol{v}^{\mathrm{ref}} - \boldsymbol{n}^{\mathrm{q}} \cdot \boldsymbol{q}) \cdot \cos\boldsymbol{\delta}\right] \\ 0^{n\mathrm{g}-1} & 0^{n\mathrm{g}-1} \end{bmatrix} \tag{11}$$

$$\frac{\partial \mathbf{g}}{\partial \boldsymbol{x}} = \begin{bmatrix} 0^{n_{\mathrm{g}}} & (\check{\boldsymbol{G}} \cdot [\boldsymbol{n}^{\mathrm{q}} \cdot \cos\boldsymbol{\delta}]^{n^{\mathrm{g}}} - \check{\boldsymbol{B}} \cdot [\boldsymbol{n}^{\mathrm{q}} \cdot \sin\boldsymbol{\delta}]^{n^{\mathrm{g}}}) & \check{\boldsymbol{G}} \cdot [(\boldsymbol{v}^{\mathrm{ref}} - \boldsymbol{n}^{\mathrm{q}} \cdot \boldsymbol{q}) \cdot \sin\boldsymbol{\delta}]^{n^{\mathrm{g}}} + \check{\boldsymbol{B}}[(\boldsymbol{v}^{\mathrm{ref}} - \boldsymbol{n}^{\mathrm{q}} \cdot \boldsymbol{q}) \cdot \cos\boldsymbol{\delta}]^{n^{\mathrm{g}}} \\ 0^{n_{\mathrm{g}}} & (\check{\boldsymbol{G}} \cdot [\boldsymbol{n}^{\mathrm{q}} \cdot \sin\boldsymbol{\delta}]^{n^{\mathrm{g}}} + \check{\boldsymbol{B}} \cdot [\boldsymbol{n}^{\mathrm{q}} \cdot \cos\boldsymbol{\delta}]^{n^{\mathrm{g}}}) & \check{\boldsymbol{B}} \cdot [(\boldsymbol{v}^{\mathrm{ref}} - \boldsymbol{n}^{\mathrm{q}} \cdot \boldsymbol{q}) \cdot \sin\boldsymbol{\delta}]^{n^{\mathrm{g}}} - \check{\boldsymbol{G}}[(\boldsymbol{v}^{\mathrm{ref}} - \boldsymbol{n}^{\mathrm{q}} \cdot \boldsymbol{q}) \cdot \cos\boldsymbol{\delta}]^{n^{\mathrm{g}}} \end{bmatrix} \tag{12}$$

$$\frac{\partial \mathbf{g}}{\partial \boldsymbol{z}} = \begin{bmatrix} I^{n^{\mathrm{g}}} + \check{\boldsymbol{G}} \cdot [\boldsymbol{r_c}]^{n^{\mathrm{g}}} - \check{\boldsymbol{B}} \cdot [\boldsymbol{x_c}]^{n^{\mathrm{g}}} & -\check{\boldsymbol{G}} \cdot [\boldsymbol{x_c}]^{n^{\mathrm{g}}} - \check{\boldsymbol{B}} \cdot [\boldsymbol{r_c}]^{n^{\mathrm{g}}} \\ \check{\boldsymbol{B}} \cdot [\boldsymbol{r_c}]^{n^{\mathrm{g}}} + \check{\boldsymbol{G}} \cdot [\boldsymbol{x_c}]^{n^{\mathrm{g}}} & I^{n^{\mathrm{g}}} + \check{\boldsymbol{G}} \cdot [\boldsymbol{r_c}]^{n^{\mathrm{g}}} - \check{\boldsymbol{B}} \cdot [\boldsymbol{x_c}]^{n^{\mathrm{g}}} \end{bmatrix} \tag{13}$$

Using (24c), an auxiliary matrix for each inverter, $\boldsymbol{X}_k \in \mathbb{S}^{n_u}\ \forall\ k \in \mathcal{G}$, is defined as

$$\boldsymbol{X}_k \triangleq \boldsymbol{u}_k \boldsymbol{u}_k^{\top}, \tag{24d}$$

that satisfies a set of constraints $\mathcal{U}$ given as

$$(\boldsymbol{e}_k^{\delta^{\mathrm{s}}})^{\top} \boldsymbol{X}_k \boldsymbol{e}_k^{q} - \delta_k^{\mathrm{qs}} = 0, \tag{25a}$$
$$(\boldsymbol{e}_k^{\delta^{\mathrm{c}}})^{\top} \boldsymbol{X}_k \boldsymbol{e}_k^{q} - \delta_k^{\mathrm{qc}} = 0, \tag{25b}$$
$$(\boldsymbol{e}_k^{\delta^{\mathrm{c}}})^{\top} \boldsymbol{X}_k \boldsymbol{e}_k^{\delta^{\mathrm{qs}}} - (\boldsymbol{e}_k^{\delta^{\mathrm{s}}})^{\top} \boldsymbol{X}_k \boldsymbol{e}_k^{\delta^{\mathrm{qc}}} = 0, \tag{25c}$$
$$(\boldsymbol{e}_k^{\delta^{\mathrm{c}}})^{\top} \boldsymbol{X}_k \boldsymbol{e}_k^{\delta^{\mathrm{c}}} + (\boldsymbol{e}_k^{\delta^{\mathrm{s}}})^{\top} \boldsymbol{X}_k \boldsymbol{e}_k^{\delta^{\mathrm{s}}} - 1 = 0, \tag{25d}$$
$$(\boldsymbol{e}_k^{\delta^{\mathrm{c}}})^{\top} \boldsymbol{X}_k \boldsymbol{e}_k^{\delta^{\mathrm{qc}}} + (\boldsymbol{e}_k^{\delta^{\mathrm{s}}})^{\top} \boldsymbol{X}_k \boldsymbol{e}^{\delta_k^{\mathrm{qs}}} - q_k = 0, \tag{25e}$$
$$(\boldsymbol{e}_k^{\delta^{\mathrm{qc}}})^{\top} \boldsymbol{X}_k \boldsymbol{e}_k^{\delta^{\mathrm{qc}}} + (\boldsymbol{e}_k^{\delta^{\mathrm{qs}}})^{\top} \boldsymbol{X}_k \boldsymbol{e}_k^{\delta^{\mathrm{qs}}} - (\boldsymbol{e}_k^{q})^{\top} \boldsymbol{X}_k \boldsymbol{e}_k^{q} = 0. \tag{25f}$$

$\boldsymbol{e}_k^{i^{\mathrm{od}}}$, $\boldsymbol{e}_k^{i^{\mathrm{od}}}$, $\boldsymbol{e}_k^{\delta^{\mathrm{c}}}$, $\boldsymbol{e}_k^{\delta^{\mathrm{s}}}$, $\boldsymbol{e}_k^{q}$, $\boldsymbol{e}_k^{\delta^{\mathrm{qc}}}$, and $\boldsymbol{e}_k^{\delta^{\mathrm{qs}}}$ are the standard basis for respective elements of the vector $\boldsymbol{u}_k$.

From (23)-(24d), the constraints (1b)-(1g), (20), (22) and sub-matrices $\boldsymbol{A}(\boldsymbol{i}^{\mathrm{od}}, \boldsymbol{i}^{\mathrm{oq}}, \boldsymbol{\delta}, \boldsymbol{q})$, $\boldsymbol{B}(\boldsymbol{\delta}, \boldsymbol{q})$, and $\boldsymbol{C}(\boldsymbol{\delta}, \boldsymbol{q})$ can be written as the linear functions of $\boldsymbol{u}_k$, and $\boldsymbol{X}_k$ as in (27), (28), (29), and (30). The state matrix $\hat{\boldsymbol{A}}$ and the stability constraint (19a) are still non-linear due to the presence of $\boldsymbol{B}\,(\boldsymbol{D})^{-1}\,\boldsymbol{C}$, $\hat{\boldsymbol{A}}^{\top}\,\boldsymbol{M}$, and $\boldsymbol{M}\hat{\boldsymbol{A}}$ terms. To overcome this, two auxiliary matrices, $\boldsymbol{E}$ and $\boldsymbol{L}$, are defined

$$\boldsymbol{E} = \begin{bmatrix} \boldsymbol{E}^{\mathrm{bb}} & \boldsymbol{E}^{\mathrm{bc}} \\ \boldsymbol{E}^{\mathrm{cb}} & \boldsymbol{E}^{\mathrm{cc}} \end{bmatrix} \triangleq \begin{bmatrix} \boldsymbol{B}(\boldsymbol{\delta}^{\mathrm{c}}, \boldsymbol{\delta}^{\mathrm{s}}, \boldsymbol{\delta}^{\mathrm{qc}}, \boldsymbol{\delta}^{\mathrm{qs}}) \\ \hat{\boldsymbol{C}}^{\top}(\boldsymbol{\delta}^{\mathrm{c}}, \boldsymbol{\delta}^{\mathrm{s}}, \boldsymbol{\delta}^{\mathrm{qc}}, \boldsymbol{\delta}^{\mathrm{qs}}) \end{bmatrix} \begin{bmatrix} \boldsymbol{B}(\boldsymbol{\delta}^{\mathrm{c}}, \boldsymbol{\delta}^{\mathrm{s}}, \boldsymbol{\delta}^{\mathrm{qc}}, \boldsymbol{\delta}^{\mathrm{qs}}) \\ \hat{\boldsymbol{C}}^{\top}(\boldsymbol{\delta}^{\mathrm{c}}, \boldsymbol{\delta}^{\mathrm{s}}, \boldsymbol{\delta}^{\mathrm{qc}}, \boldsymbol{\delta}^{\mathrm{qs}}) \end{bmatrix}^{\top} \tag{26a}$$

$$\boldsymbol{L} = \begin{bmatrix} \boldsymbol{L}^{\mathrm{mm}} & \boldsymbol{L}^{\mathrm{ma}} \\ \boldsymbol{L}^{\mathrm{am}} & \boldsymbol{L}^{\mathrm{aa}} \end{bmatrix} \triangleq \begin{bmatrix} \boldsymbol{M} \\ \hat{\boldsymbol{A}}^{\top} \end{bmatrix} [\boldsymbol{M}, \hat{\boldsymbol{A}}], \tag{26b}$$

where $\hat{\boldsymbol{C}}(\boldsymbol{\delta}^{\mathrm{c}}, \boldsymbol{\delta}^{\mathrm{s}}, \boldsymbol{\delta}^{\mathrm{qc}}, \boldsymbol{\delta}^{\mathrm{qs}}) = (\boldsymbol{D})^{-1}\boldsymbol{C}(\boldsymbol{\delta}^{\mathrm{c}}, \boldsymbol{\delta}^{\mathrm{s}}, \boldsymbol{\delta}^{\mathrm{qc}}, \boldsymbol{\delta}^{\mathrm{qs}})$. $\boldsymbol{D}$ is a constant matrix for a given distribution network.

The lifted formulation of the SCOPF is given in (27), where (27b)-(27l) are linear and convex. The non-convexity present in the original SCOPF is encapsulated by the constraints (27o)-(27r).

B. Convex Relaxation

To ensure that (27) is computationally tractable, non-convex constraints (27o)- (27r) are relaxed. This paper details two distinct relaxation approaches, a SDP relaxation and a computationally-efficient parabolic relaxation.

1) SDP relaxation: The SDP relaxation of the non-convex constraints in the lifted SCOPF problem (27) is given as

$$\boldsymbol{W} - \boldsymbol{v}\boldsymbol{v}^{*} \succeq 0, \tag{31a}$$
$$\begin{bmatrix} \boldsymbol{E}^{\mathrm{bb}} & \boldsymbol{E}^{\mathrm{bc}} \\ \boldsymbol{E}^{\mathrm{cb}} & \boldsymbol{E}^{\mathrm{cc}} \end{bmatrix} - \begin{bmatrix} \boldsymbol{B}(\boldsymbol{\delta}^{\mathrm{c}}, \boldsymbol{\delta}^{\mathrm{s}}, \boldsymbol{\delta}^{\mathrm{qc}}, \boldsymbol{\delta}^{\mathrm{qs}}) \\ \hat{\boldsymbol{C}}^{\top}(\boldsymbol{\delta}^{\mathrm{c}}, \boldsymbol{\delta}^{\mathrm{s}}, \boldsymbol{\delta}^{\mathrm{qc}}, \boldsymbol{\delta}^{\mathrm{qs}}) \end{bmatrix} \begin{bmatrix} \boldsymbol{B}(\boldsymbol{\delta}^{\mathrm{c}}, \boldsymbol{\delta}^{\mathrm{s}}, \boldsymbol{\delta}^{\mathrm{qc}}, \boldsymbol{\delta}^{\mathrm{qs}}) \\ \hat{\boldsymbol{C}}^{\top}(\boldsymbol{\delta}^{\mathrm{c}}, \boldsymbol{\delta}^{\mathrm{s}}, \boldsymbol{\delta}^{\mathrm{qc}}, \boldsymbol{\delta}^{\mathrm{qs}}) \end{bmatrix}^{\top} \succeq 0, \tag{31b}$$
$$\begin{bmatrix} \boldsymbol{L}^{\mathrm{mm}} & \boldsymbol{L}^{\mathrm{ma}} \\ \boldsymbol{L}^{\mathrm{am}} & \boldsymbol{L}^{\mathrm{aa}} \end{bmatrix} - \begin{bmatrix} \boldsymbol{M} \\ \hat{\boldsymbol{A}}^{\top} \end{bmatrix} [\boldsymbol{M}, \hat{\boldsymbol{A}}] \succeq 0, \tag{31c}$$
$$\boldsymbol{X}_k - \boldsymbol{u}_k \boldsymbol{u}_k{}^{\top} \succeq 0 \quad \forall\ k \in \mathcal{G}. \tag{31d}$$

Remark 1. *The constraints (31a)-(31d) can be cast as*

$$\begin{bmatrix} \boldsymbol{W} & \boldsymbol{v} \\ \boldsymbol{v}^{*} & 1 \end{bmatrix} \succeq 0, \tag{32}$$
$$\begin{bmatrix} \boldsymbol{E}^{\mathrm{bb}} & \boldsymbol{E}^{\mathrm{bc}} & \boldsymbol{B}^{\top}(\boldsymbol{\delta}^{\mathrm{c}}, \boldsymbol{\delta}^{\mathrm{s}}, \boldsymbol{\delta}^{\mathrm{qc}}, \boldsymbol{\delta}^{\mathrm{qs}}) \\ \boldsymbol{E}^{\mathrm{cb}} & \boldsymbol{E}^{\mathrm{cc}} & \hat{\boldsymbol{C}}^{\top}(\boldsymbol{\delta}^{\mathrm{c}}, \boldsymbol{\delta}^{\mathrm{s}}, \boldsymbol{\delta}^{\mathrm{qc}}, \boldsymbol{\delta}^{\mathrm{qs}}) \\ \boldsymbol{B}^{\top}(\boldsymbol{\delta}^{\mathrm{c}}, \boldsymbol{\delta}^{\mathrm{s}}, \boldsymbol{\delta}^{\mathrm{qc}}, \boldsymbol{\delta}^{\mathrm{qs}}) & \hat{\boldsymbol{C}}(\boldsymbol{\delta}^{\mathrm{c}}, \boldsymbol{\delta}^{\mathrm{s}}, \boldsymbol{\delta}^{\mathrm{qc}}, \boldsymbol{\delta}^{\mathrm{qs}}) & \mathbf{I}^{n_z} \end{bmatrix} \succeq 0, \tag{33}$$
$$\begin{bmatrix} \boldsymbol{L}^{\mathrm{mm}} & \boldsymbol{L}^{\mathrm{ma}} & \boldsymbol{M} \\ \boldsymbol{L}^{\mathrm{am}} & \boldsymbol{L}^{\mathrm{aa}} & \hat{\boldsymbol{A}}^{\top} \\ \boldsymbol{M} & \hat{\boldsymbol{A}} & \mathbf{I}^{n_x} \end{bmatrix} \succeq 0, \tag{34}$$
$$\begin{bmatrix} \boldsymbol{X}_k & \boldsymbol{u}_k \\ \boldsymbol{u}_k^{\top} & 1 \end{bmatrix} \succeq 0, \qquad \forall k \in \mathcal{G}. \tag{35}$$

The above remark transforms the quadratic matrix inequalities (31b)-(31d) to convex linear matrix inequalities making the SCOPF more tractable. Nevertheless, with the increase in number of inverters and system size, solving SCOPF in (27) may become computationally challenging.

2) Parabolic relaxation: This is an alternative relaxation technique with a reduced computational burden. The non-convex problem is transformed to a convex quadratic constraint quadratic programming problem. The parabolic relaxation [20] of the non-convex voltage constraint, (27o), is given by

$$|v_j + v_k|^2 \leq W_{jj} + W_{kk} + (W_{kj} + W_{jk})\ \forall (j,k) \in \mathcal{L} \tag{36a}$$
$$|v_j - v_k|^2 \leq W_{jj} + W_{kk} - (W_{kj} + W_{jk})\ \forall (j,k) \in \mathcal{L} \tag{36b}$$
$$|v_j + \mathrm{j}v_k|^2 \leq W_{jj} + W_{kk} - \mathrm{j}(W_{kj} - W_{jk})\ \forall (j,k) \in \mathcal{L} \tag{36c}$$
$$|v_j - \mathrm{j}v_k|^2 \leq W_{jj} + W_{kk} + \mathrm{j}(W_{kj} - W_{jk})\ \forall (j,k) \in \mathcal{L} \tag{36d}$$
$$|v_j|^2 \leq W_{jj} \qquad \forall j \in \mathcal{N}. \tag{36e}$$

The parabolic relaxation of (27p)-(27r) can be obtained using the following proposition.

$$\text{minimize} \quad \mathrm{h}(\boldsymbol{p}^{\mathrm{g}}) \tag{27a}$$

subject to

OPF constraints:

$$\boldsymbol{G}^{\top}(\boldsymbol{p}+j\boldsymbol{q}) = \boldsymbol{d} + \mathrm{diag}\{\boldsymbol{W}\boldsymbol{Y}^{*}\} \tag{27b}$$

$$\mathrm{diag}\{\vec{\boldsymbol{L}}\,\boldsymbol{W}\vec{\boldsymbol{Y}}^{*}\} \le \boldsymbol{f}^{\max} \tag{27c}$$

$$\mathrm{diag}\{\overleftarrow{\boldsymbol{L}}\,\boldsymbol{W}\overleftarrow{\boldsymbol{Y}}^{*}\} \le \boldsymbol{f}^{\max} \tag{27d}$$

$$\boldsymbol{p}^{\min} \le \boldsymbol{p} \le \boldsymbol{p}^{\max} \tag{27e}$$

$$\boldsymbol{q}^{\min} \le \boldsymbol{q} \le \boldsymbol{q}^{\max} \tag{27f}$$

$$(\boldsymbol{v}^{\min})^2 \le \mathrm{diag}(\boldsymbol{W}) \le (\boldsymbol{v}^{\max})^2 \tag{27g}$$

$$\boldsymbol{i}^{\mathrm{o}} = \boldsymbol{G}^{\top}\boldsymbol{Y}\boldsymbol{v} \tag{27h}$$

$$\boldsymbol{G}^{\top}\boldsymbol{v} = \boldsymbol{v}^{\mathrm{ref}} \cdot (\boldsymbol{\delta}^{\mathrm{c}} + \mathrm{j}\boldsymbol{\delta}^{\mathrm{s}}) - \boldsymbol{n}^{q} \cdot (\boldsymbol{\delta}^{\mathrm{qc}} + \mathrm{j}\boldsymbol{\delta}^{\mathrm{qs}}) - \boldsymbol{i}^{\mathrm{o}} \cdot \boldsymbol{z}^{\mathrm{c}} \tag{27i}$$

$$p_k + \mathrm{j}q_k = ((\boldsymbol{e}_k^{i^{\mathrm{od}}})^{\top}\boldsymbol{X}_k\boldsymbol{e}_k^{i^{\mathrm{od}}} + (\boldsymbol{e}_k^{i^{\mathrm{oq}}})^{\top}\boldsymbol{X}_k\boldsymbol{e}_k^{i^{\mathrm{oq}}})z_k^{\mathrm{c}} + p_k^{g} + \mathrm{j}q_k^{g} \quad \forall\, k \in \mathcal{G} \tag{27j}$$

Stability constraints:

$$\boldsymbol{L}^{\mathrm{am}} + \boldsymbol{L}^{\mathrm{ma}} \preceq -2\eta\boldsymbol{M} \tag{27k}$$

$$\boldsymbol{M} \succeq \mathbf{I}^{n_{\mathrm{x}}} \tag{27l}$$

Auxiliary variable constraints:

$$\hat{\boldsymbol{A}} = \boldsymbol{A}(\boldsymbol{X}_k) - \boldsymbol{E} \quad \forall\, k \in \mathcal{G} \tag{27m}$$

$$\boldsymbol{u}_k = [i_k^{\mathrm{od}}, i_k^{\mathrm{oq}}, \delta_k^{\mathrm{c}}, \delta_k^{\mathrm{s}}, q_k, \delta_k^{\mathrm{qc}}, \delta_k^{\mathrm{qs}}]^{\top} \ \forall k \in \mathcal{G} \tag{27n}$$

$$\boldsymbol{W} = \boldsymbol{v}\boldsymbol{v}^{*} \tag{27o}$$

$$\begin{bmatrix}\boldsymbol{E}^{\mathrm{bb}} & \boldsymbol{E}^{\mathrm{bc}}\\ \boldsymbol{E}^{\mathrm{cb}} & \boldsymbol{E}^{\mathrm{cc}}\end{bmatrix} = \begin{bmatrix}\boldsymbol{B}(\boldsymbol{\delta}^{\mathrm{c}},\boldsymbol{\delta}^{\mathrm{s}},\boldsymbol{\delta}^{\mathrm{qc}},\boldsymbol{\delta}^{\mathrm{qs}})\\ \hat{\boldsymbol{C}}^{\top}(\boldsymbol{\delta}^{\mathrm{c}},\boldsymbol{\delta}^{\mathrm{s}},\boldsymbol{\delta}^{\mathrm{qc}},\boldsymbol{\delta}^{\mathrm{qs}})\end{bmatrix}\begin{bmatrix}\boldsymbol{B}(\boldsymbol{\delta}^{\mathrm{c}},\boldsymbol{\delta}^{\mathrm{s}},\boldsymbol{\delta}^{\mathrm{qc}},\boldsymbol{\delta}^{\mathrm{qs}})\\ \hat{\boldsymbol{C}}^{\top}(\boldsymbol{\delta}^{\mathrm{c}},\boldsymbol{\delta}^{\mathrm{s}},\boldsymbol{\delta}^{\mathrm{qc}},\boldsymbol{\delta}^{\mathrm{qs}})\end{bmatrix}^{\top} \tag{27p}$$

$$\begin{bmatrix}\boldsymbol{L}^{\mathrm{mm}} & \boldsymbol{L}^{\mathrm{ma}}\\ \boldsymbol{L}^{\mathrm{am}} & \boldsymbol{L}^{\mathrm{aa}}\end{bmatrix} = \begin{bmatrix}\boldsymbol{M}\\ \hat{\boldsymbol{A}}^{\top}\end{bmatrix}[\boldsymbol{M}\ \hat{\boldsymbol{A}}] \tag{27q}$$

$$\boldsymbol{X}_k = [i_k^{\mathrm{od}}, i_k^{\mathrm{oq}}, \delta_k^{\mathrm{c}}, \delta_k^{\mathrm{s}}, q_k, \delta_k^{\mathrm{qc}}, \delta_k^{\mathrm{qs}}]^{\top}[i_k^{\mathrm{od}}, i_k^{\mathrm{oq}}, \delta_k^{\mathrm{c}}, \delta_k^{\mathrm{s}}, q_k, \delta_k^{\mathrm{qc}}, \delta_k^{\mathrm{qs}}] \quad \forall\, k \in \mathcal{G} \tag{27r}$$

$$\boldsymbol{X}_k, [i_k^{\mathrm{od}}, i_k^{\mathrm{oq}}, \delta_k^{\mathrm{c}}, \delta_k^{\mathrm{s}}, q_k, \delta_k^{\mathrm{qc}}, \delta_k^{\mathrm{qs}}]^{\top} \in \mathcal{U} \quad \forall\, k \in \mathcal{G} \tag{27s}$$

varaibles

$\boldsymbol{v} \in \mathbb{C}^{n\times 1},\ \boldsymbol{p}^{\mathrm{g}} \in \mathbb{R}^{n^{\mathrm{g}}\times 1},\ \boldsymbol{q}^{\mathrm{g}} \in \mathbb{R}^{n^{\mathrm{g}}\times 1},\ \boldsymbol{i}^{\mathrm{o}} \in \mathbb{C}^{n^{\mathrm{g}}\times 1},$
$\boldsymbol{q} \in \mathbb{R}^{n^{\mathrm{g}}\times 1},\ \boldsymbol{\delta}^{\mathrm{c}} \in \mathbb{R}^{n^{\mathrm{g}}\times 1},\ \boldsymbol{\delta}^{\mathrm{s}} \in \mathbb{R}^{n^{\mathrm{g}}\times 1},\ \boldsymbol{\delta}^{\mathrm{qc}} \in \mathbb{R}^{n^{\mathrm{g}}\times 1},$
$\boldsymbol{\delta}^{\mathrm{qs}} \in \mathbb{R}^{n^{\mathrm{g}}\times 1},\ \boldsymbol{M} \in \mathbb{S}^{n^{\mathrm{g}}},\ \boldsymbol{W} \in \mathbb{H}^{n},\ \hat{\boldsymbol{A}} \in \mathbb{R}^{n_{\mathrm{x}}\times n_{\mathrm{x}}},$
$\boldsymbol{E} = \begin{bmatrix}\boldsymbol{E}^{\mathrm{bb}} & \boldsymbol{E}^{\mathrm{bc}}\\ \boldsymbol{E}^{\mathrm{cb}} & \boldsymbol{E}^{\mathrm{cc}}\end{bmatrix} \in \mathbb{R}^{2n_{\mathrm{x}}\times 2n_{\mathrm{x}}},\ \boldsymbol{L} = \begin{bmatrix}\boldsymbol{L}^{\mathrm{mm}} & \boldsymbol{L}^{\mathrm{ma}}\\ \boldsymbol{L}^{\mathrm{am}} & \boldsymbol{L}^{\mathrm{aa}}\end{bmatrix} \in \mathbb{R}^{2n_{\mathrm{x}}\times 2n_{\mathrm{x}}},$
and $\boldsymbol{X}_k \in \mathbb{R}^{n_u\times n_u} \forall\, k \in \mathcal{G}$.

where

$\mathcal{U}$ is set of constraints defined as (25),

The matrices $\boldsymbol{A}(\boldsymbol{X}_k)$, $\boldsymbol{B}(\boldsymbol{\delta}^{\mathrm{c}},\boldsymbol{\delta}^{\mathrm{s}},\boldsymbol{\delta}^{\mathrm{qc}},\boldsymbol{\delta}^{\mathrm{qs}})$, and $\boldsymbol{C}(\boldsymbol{\delta}^{\mathrm{c}},\boldsymbol{\delta}^{\mathrm{s}},\boldsymbol{\delta}^{\mathrm{qc}},\boldsymbol{\delta}^{\mathrm{qs}})$ are defined as (28), (29), and (30), respectively.

Proposition 2. *Assume $\boldsymbol{R} \in \mathbb{R}^{r\times s}$, $\boldsymbol{S} \in \mathbb{R}^{s\times r}$, and $\boldsymbol{T} \in \mathbb{S}^{2r}$ are the matrices expressed by*

$$\boldsymbol{T} = \begin{bmatrix}\boldsymbol{T}^{\mathrm{rr}} & \boldsymbol{T}^{\mathrm{rs}}\\ \boldsymbol{T}^{\mathrm{sr}} & \boldsymbol{T}^{\mathrm{ss}}\end{bmatrix} = [\boldsymbol{R}^{\top},\ \boldsymbol{S}]^{\top}[\boldsymbol{R}^{\top},\ \boldsymbol{S}]. \tag{36f}$$

The parabolic relaxation [21] is formulated as

$$T_{jj}^{\mathrm{rr}} + T_{kk}^{\mathrm{ss}} + 2T_{jk}^{\mathrm{rs}} \ge \|\boldsymbol{r}_j + \boldsymbol{s}_k\|^2 \ \ \forall j,k \in \{1,2,..,r\}, \tag{36g}$$

$$T_{jj}^{\mathrm{rr}} + T_{kk}^{\mathrm{ss}} - 2T_{jk}^{\mathrm{rs}} \ge \|\boldsymbol{r}_j - \boldsymbol{s}_k\|^2 \ \ \forall j,k \in \{1,2,..,r\}. \tag{36h}$$

Here, $\boldsymbol{r}_j$ and $\boldsymbol{s}_k$ are the j^{th} and k^{th} column vectors of the matrices $\boldsymbol{R}$ and $\boldsymbol{S}^{\top}$, respectively.

While the relaxed SCOPF problem is computationally tractable, it may not guarantee a feasible globally optimal solution for the original problem in (1). Therefore, a sequential penalization approach is adopted.

C. Sequential Penalization

The solution obtained from the lifted problem (27a)-(27m) with the relaxed SCOPF constraints (32)-(35) or (36a)-(36h) may not be always feasible with the original problem (1). To resolve this, the SCOPF is modified by adding a linear penalty function ρ to the objective function in (27a)

$$\text{minimize } \mathrm{h}(\boldsymbol{p}^{\mathrm{g}}) + \rho(\boldsymbol{W},\boldsymbol{v},\boldsymbol{E},\boldsymbol{B},\hat{\boldsymbol{C}},\boldsymbol{L},\boldsymbol{M},\hat{\boldsymbol{A}},\boldsymbol{X},\boldsymbol{u}) \tag{37a}$$

$$\text{subject to (27b)-(27m)}, \tag{37b}$$

$$\text{(32)-(35) SDP relaxed constraints,} \tag{37c}$$

$$\text{or}$$

$$\text{(36a)-(36h) Parabolic relaxed constraints,} \tag{37d}$$

where

$$\rho(\boldsymbol{W},\boldsymbol{v},\boldsymbol{E},\boldsymbol{B},\hat{\boldsymbol{C}},\boldsymbol{L},\boldsymbol{M},\hat{\boldsymbol{A}},\boldsymbol{X},\boldsymbol{u}) \tag{38}$$

$$\begin{aligned}\triangleq\ & (\mathrm{tr}\{\boldsymbol{W}\boldsymbol{P}\} - \boldsymbol{v}_0^{*}\boldsymbol{P}\boldsymbol{v} - \boldsymbol{v}^{*}\boldsymbol{P}\boldsymbol{v}_0 + \boldsymbol{v}_0^{*}\boldsymbol{P}\boldsymbol{v}_0) + \mu_1(\mathrm{tr}\{\boldsymbol{E}\} - \\ & 2\mathrm{tr}\{\boldsymbol{B}_0\boldsymbol{B}^{\top}\} - 2\mathrm{tr}\{\hat{\boldsymbol{C}}_0\hat{\boldsymbol{C}}^{\top}\} + \mathrm{tr}\{\boldsymbol{B}_0\boldsymbol{B}_0^{\top}\} + \mathrm{tr}\{\hat{\boldsymbol{C}}_0\hat{\boldsymbol{C}}_0^{\top}\}) \\ & \mu_2(\mathrm{tr}\{\boldsymbol{L}\} - 2\mathrm{tr}\{\boldsymbol{M}_0\boldsymbol{M}^{\top}\} - 2\mathrm{tr}\{\hat{\boldsymbol{A}}_0\hat{\boldsymbol{A}}^{\top}\} + \mathrm{tr}\{\boldsymbol{M}_0\boldsymbol{M}_0^{\top}\} \\ & + \mathrm{tr}\{\hat{\boldsymbol{A}}_0\hat{\boldsymbol{A}}_0^{\top}\}) + \mu_3\mathrm{tr}\{\boldsymbol{X}_k - 2\boldsymbol{u}_{0_k}\boldsymbol{u}_k^{\top} + \boldsymbol{u}_{0_k}\boldsymbol{u}_{0_k}^{\top}\}.\end{aligned} \tag{39}$$

$\boldsymbol{v}_0, \boldsymbol{B}_0, \hat{\boldsymbol{C}}_0, \boldsymbol{M}_0, \hat{\boldsymbol{A}}_0, \boldsymbol{u}_{0_k}$ are the given initial values. μ_1, μ_2, and μ_3 are the penalty positive coefficients valued at 0.1, 0.5, and 5, respectively. Here, $\boldsymbol{P}$ is the penalty function coefficient matrix for the voltage which can be calculated as in [20]. For an arbitrary initial point, the SCOPF (37) is solved sequentially until a feasible solution to (1) is obtained. It can then reduce the value of the objective function in subsequent iterations until a (near) global optimal solution is found [22].

V. Validation and Verification

A. Numerical Studies

The efficacy of both SDP and parabolic convex relaxations are evaluated on several standard test systems. All numerical studies are performed using MATLAB/CVX platform on a 64-bit personal computer with 3.4GHz Intel i7 quadcore processor and 64 GB RAM. The droop constants $\boldsymbol{m}^{\mathrm{p}} = 1.5\times10^{-4}$ and $\boldsymbol{n}^{\mathrm{q}} = 7.2\times10^{-4}$ are chosen. In Table I, upper bound (UB) indicates the globally optimal cost obtained after sequential penalization, Lower bound (LB) indicates the optimal cost

TABLE I: Upper bounds, lower bounds, and computational times for SCOPF with SDP and parabolic relaxations.

Test system	n^{g}	UB	SDP		Parabolic	
			LB	time (s)	LB	time (s)
9-bus	3	4234.76	3984.51	0.44	3900.42	0.42
14-bus	5	7963.32	7076.86	0.61	6561.84	0.53
30-bus	6	563.15	523.77	0.95	498.90	0.61
57-bus	7	43728.37	39803.98	2.88	35740.58	1.26
39-bus	10	39241.56	33307.43	6.83	32607.87	3.33
89pegase	12	5830.64	5127.92	19.95	4226.49	8.69
24_ieee_rts	33	-	56877.63	3487.61	53263.30	728.30

$$\boldsymbol{A} = \begin{bmatrix} -[\boldsymbol{\omega}^{\mathrm{c}}] & -\left[\left(\omega_k^{\mathrm{c}} n_k^{\mathrm{q}}((\boldsymbol{e}_k^{i^{\mathrm{oq}}})^\top \boldsymbol{X}_k \boldsymbol{e}_k^{\delta^{\mathrm{s}}} + (\boldsymbol{e}_k^{i^{\mathrm{od}}})^\top \boldsymbol{X}_k \boldsymbol{e}_k^{\delta^{\mathrm{c}}})\right)_{k\in\mathcal{G}}\right] & -\left[\left(\omega_k^{\mathrm{c}}(v_k^{\mathrm{ref}}((\boldsymbol{e}_k^{i^{\mathrm{oq}}})^\top \boldsymbol{X}_k \boldsymbol{e}_k^{\delta^{\mathrm{s}}} + (\boldsymbol{e}_k^{i^{\mathrm{od}}})^\top \boldsymbol{X}_k \boldsymbol{e}_k^{\delta^{\mathrm{c}}}))\right)_{k\in\mathcal{G}}\right] + \\ & & \left[\left(\omega_k^{\mathrm{c}} n_k^{\mathrm{q}}(((\boldsymbol{e}_k^{i^{\mathrm{oq}}})^\top \boldsymbol{X}_k \boldsymbol{e}_k^{\delta^{\mathrm{qs}}} + (\boldsymbol{e}_k^{i^{\mathrm{od}}})^\top \boldsymbol{X}_k \boldsymbol{e}_k^{\delta^{\mathrm{qc}}}))\right)_{k\in\mathcal{G}}\right] \\ 0^{n^{\mathrm{g}}} & \left[\left(\omega_k^{\mathrm{c}} n_k^{\mathrm{q}}((\boldsymbol{e}_k^{i^{\mathrm{oq}}})^\top \boldsymbol{X}_k \boldsymbol{e}_k^{\delta^{\mathrm{c}}} - (\boldsymbol{e}_k^{i^{\mathrm{od}}})^\top \boldsymbol{X}_k \boldsymbol{e}_k^{\delta^{\mathrm{s}}}) - \omega_k^{\mathrm{c}}\right)_{k\in\mathcal{G}}\right] & \left[\left(\omega_k^{\mathrm{c}}(v_k^{\mathrm{ref}}((\boldsymbol{e}_k^{i^{\mathrm{od}}})^\top \boldsymbol{X}_k \boldsymbol{e}_k^{\delta^{\mathrm{c}}} + (\boldsymbol{e}_k^{i^{\mathrm{oq}}})^\top \boldsymbol{X}_k \boldsymbol{e}_k^{\delta^{\mathrm{s}}}))\right)_{k\in\mathcal{G}}\right] - \\ & & \left[\left(\omega_k^{\mathrm{c}} n_k^{\mathrm{q}}(((\boldsymbol{e}_k^{i^{\mathrm{od}}})^{\mathrm{I}} \boldsymbol{X}_k \boldsymbol{e}_k^{\delta^{\mathrm{qc}}} + (\boldsymbol{e}_k^{i^{\mathrm{oq}}})^{\mathrm{I}} \boldsymbol{X}_k \boldsymbol{e}_k^{\delta^{\mathrm{qs}}}))\right)_{k\in\mathcal{G}}\right] \\ \boldsymbol{M}^{\mathrm{p}} & 0^{n^{\mathrm{g}}-1} & 0^{n^{\mathrm{g}}-1} \end{bmatrix} \tag{28}$$

$$\boldsymbol{B} = \begin{bmatrix} \left[\left(\omega_k^{\mathrm{c}}(v_k^{\mathrm{ref}}\delta_k^{\mathrm{c}} - n_k^{\mathrm{q}}\delta_k^{\mathrm{qc}})\right)_{k\in\mathcal{G}}\right] & \left[\left(\omega_k^{\mathrm{c}}(v_k^{\mathrm{ref}}\delta_k^{\mathrm{s}} - n_k^{\mathrm{q}}\delta_k^{\mathrm{qs}})\right)_{k\in\mathcal{G}}\right] \\ \left[\left(\omega_k^{\mathrm{c}}(v_k^{\mathrm{ref}}\delta_k^{\mathrm{s}} - n_k^{\mathrm{q}}\delta_k^{\mathrm{qs}})\right)_{k\in\mathcal{G}}\right] & -\left[\left(\omega_k^{\mathrm{c}}(v_k^{\mathrm{ref}}\delta_k^{\mathrm{c}}) - n_k^{\mathrm{q}}\delta_k^{\mathrm{qc}})\right)_{k\in\mathcal{G}}\right] \\ 0^{n\mathrm{g}-1} & 0^{n\mathrm{g}-1} \end{bmatrix} \tag{29}$$

$$\hat{\boldsymbol{C}} = \boldsymbol{D}^{-1}\begin{bmatrix} 0^{n_{\mathrm{g}}} & \check{\boldsymbol{G}}\cdot[(n_k^{\mathrm{q}}\delta_k^{\mathrm{c}})_{k\in\mathcal{G}}]^{n^{\mathrm{g}}} - \check{\boldsymbol{B}}\cdot[(n_k^{\mathrm{q}}\delta_k^{\mathrm{s}})_{k\in\mathcal{G}}]^{n^{\mathrm{g}}} & \check{\boldsymbol{G}}\cdot[(v_k^{\mathrm{ref}}\delta_k^{\mathrm{s}} - n_k^{\mathrm{q}}\delta_k^{\mathrm{qs}})_{k\in\mathcal{G}}]^{n^{\mathrm{g}}} + \check{\boldsymbol{B}}\cdot[(v^{\mathrm{ref}_k}\delta_k^{\mathrm{c}} - n_k^{\mathrm{q}}\delta_k^{\mathrm{qc}})_{k\in\mathcal{G}}]^{n^{\mathrm{g}}} \\ 0^{n_{\mathrm{g}}} & \check{\boldsymbol{G}}\cdot[(n_k^{\mathrm{q}}\delta_k^{\mathrm{s}})_{k\in\mathcal{G}}]^{n^{\mathrm{g}}} + \check{\boldsymbol{B}}\cdot[(n_k^{\mathrm{q}}\delta_k^{\mathrm{c}})_{k\in\mathcal{G}}]^{n^{\mathrm{g}}} & \check{\boldsymbol{B}}\cdot[(v_k^{\mathrm{ref}}\delta_k^{\mathrm{s}} - n_k^{\mathrm{q}}\delta_k^{\mathrm{qs}})_{k\in\mathcal{G}}]^{n^{\mathrm{g}}} - \check{\boldsymbol{G}}[(v^{\mathrm{ref}_k}\delta_k^{\mathrm{c}} - n_k^{\mathrm{q}}\delta_k^{\mathrm{qc}})_{k\in\mathcal{G}}]^{n^{\mathrm{g}}} \end{bmatrix} \tag{30}$$

obtained for the relaxed problem without penalty, and computational time indicates the time taken by the optimization solver to solve the relaxed problem without sequential penalization. From Table I, for smaller systems with less number of inverters, the SDP relaxation offers LBs closer to the global solution with similar computational time as compared to parabolic relaxation. As the number of inverters and system size increases, SDP becomes computationally more expensive.

B. Hardware-in-the-Loop Validation

The proposed SCOPF is tested on a 4-bus,4-inverter microgrid system [23], shown in Fig. 2. Inverters power limits and their cost coefficients are detailed in Table II. The microgrid's base power and voltage are $0.1MVA$ and $480V$, respectively.

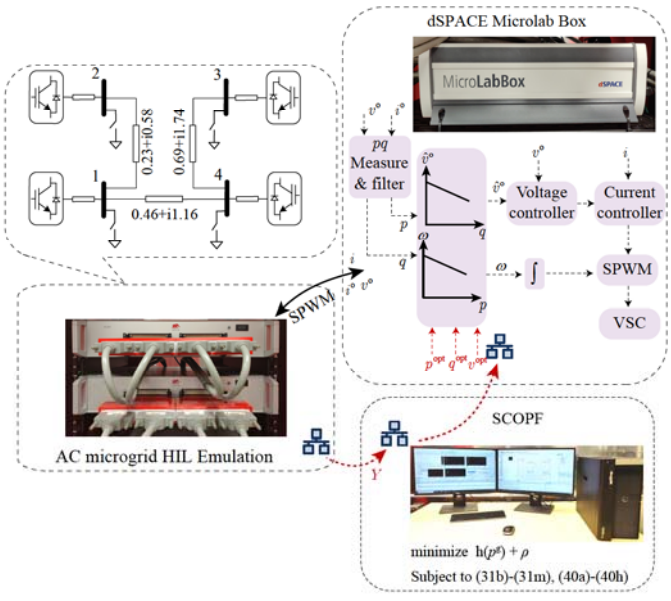

Fig. 2: The microgrid test system implemented using HIL (Typhoon HIL), control unit (dSPACE), and optimization unit (personal computer), with information flow shown.

The nominal frequency of the microgrid is $\omega_{\mathrm{nom}} = 377rad/s$. This microgrid has variable-impedance loads, with 0.707 lagging power factor, at all buses. The complete microgrid is emulated in two Typhoon HIL604 units. The stability constraint threshold in SCOPF is chosen as $\eta = 0.1$. Inverters employ droop control schemes with $\boldsymbol{m}^{\mathrm{p}} = 1.04 \times 10^{-4}$ and $\boldsymbol{n}^{\mathrm{q}} = 2.3 \times 10^{-4}$. These controllers are realized using two dSPACE MLBx control boxes. A personal computer (PC) with a 8-core, 3.5GHz Xeon processor, and 64GB RAM solves the SCOPF using MATLAB/CVX optimization tool, and provides the optimal set-point information to the dSPACE.

1) Microgrid performance without and with SCOPF: The microgrid system is emulated in the HIL environment for 30 minutes. Every 20 seconds, loads at all buses are randomly varied following a poisson distribution. Figures 3 and 4 depict the microgrid operation without and with SCOPF, respectively. Without SCOPF, the set-point values were held constant at $\boldsymbol{p}^{\mathrm{opt}} = 0$, $\boldsymbol{q}^{\mathrm{opt}} = 0$, and $\boldsymbol{v}^{\mathrm{opt}} = 480V$. The voltages and the reactive power generations are within the limits for both scenarios, as shown in Fig. 3(c),(d) and Fig. 4(c),(d). The active power load variations are shared equally among all the inverters due to the constant active power set-point ($\boldsymbol{p}^{\mathrm{opt}}$) and identical droop constants ($\boldsymbol{m}^{\mathrm{p}}$), as shown in Fig. 3(b). On the contrary, using SCOPF, the optimal set-points are provided at every 2 minutes, leading to unequal, but cost effective powers supplied by the inverters, as shown in Fig. 4(b). The average total generation cost for 30 minutes, with the droop control alone, is 253.5723. Using SCOPF, the average total generation cost reduces to 233.7836. Moreover, it can be observed from Fig. 3(a) and 4(a) that the operating frequency, with the droop control alone, deviates further from the nominal value (ω_{nom}) compared to when SCOPF is employed.

TABLE II: Generational cost coefficients and power limits

Bus	c_2	c_1	c_0	$p^{\min}$	$p^{\max}$	$q^{\min}$	$q^{\max}$
1	1.3	2.2	0	0	1.0	-0.80	0.80
2	1.6	2.8	0	0	1.0	-0.80	0.80
3	2.0	5.5	0	0	1.0	-0.80	0.80
4	1.6	2.4	0	0	1.0	-0.80	0.80

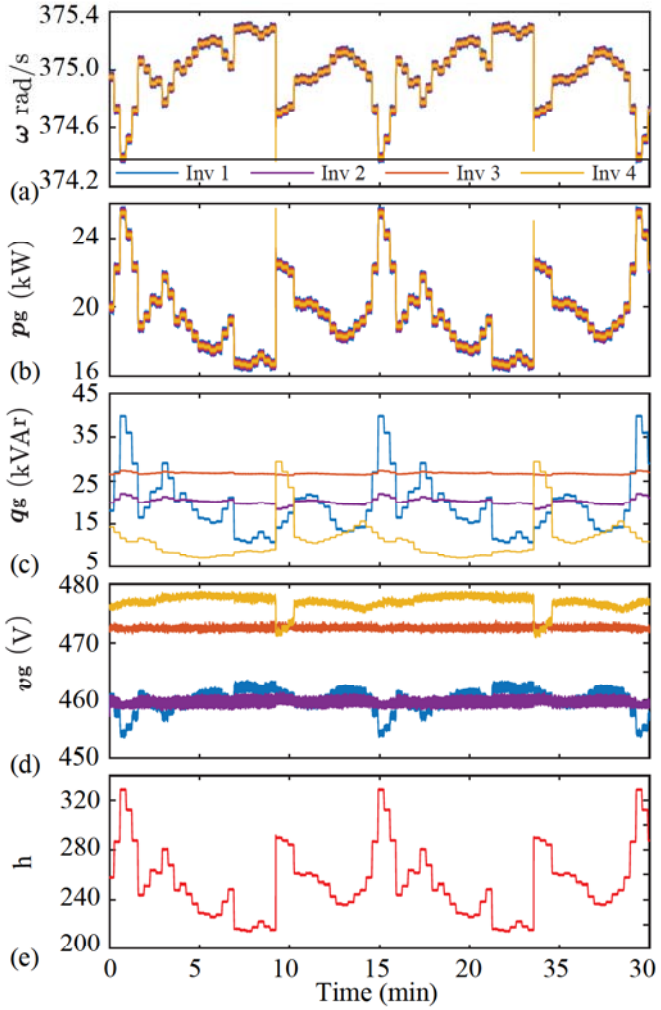

Fig. 3: Operation with droop control and varying loads at bus 1 and 4: (a) frequency, (b) active power, (c) reactive power, (d) voltage magnitude, and (e) total generation cost.

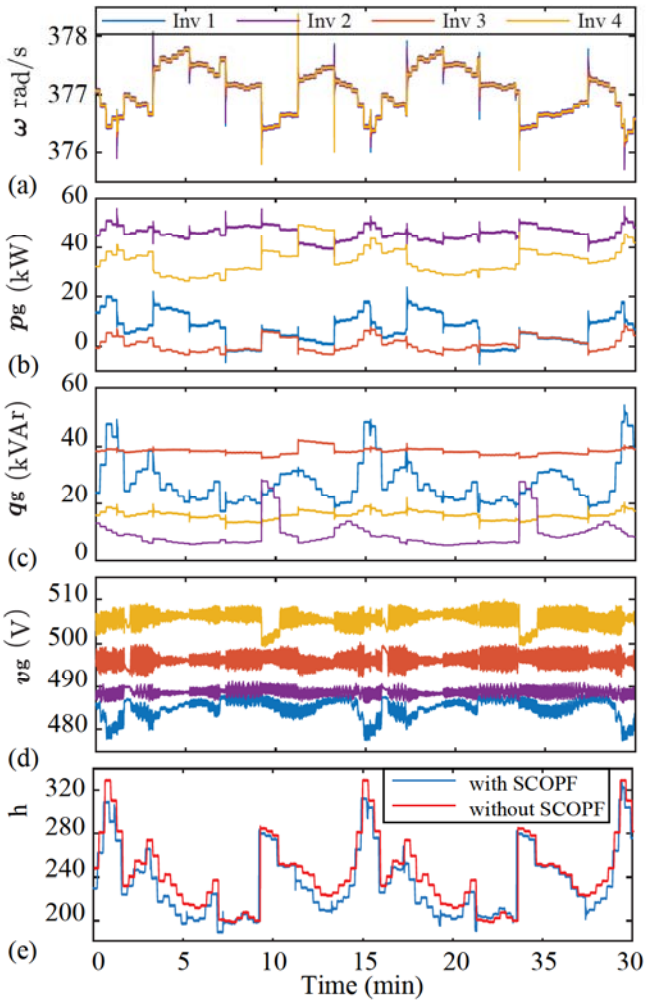

Fig. 4: Microgrid operation with SCOPF and varying loads at bus 1 and 4: (a) frequency, (b) active power, (c) reactive power, (d) voltage magnitude, and (e) total generation cost.

2) Comparing conventional OPF and SCOPF: The advantage of SCOPF over the conventional OPF is demonstrated here. Figures 5 and 6 portray the microgrid performance with the operating set-points dictated by OPF and SCOPF, respectively. In both scenarios, initially, the microgrid operates with load impedance of $(5+i5)\ \Omega$ at all buses. At $t = t_1$, the load at bus 3 is disconnected. Set-points provided by SCOPF lead to better damping as compared to that of conventional OPF, as observed from Fig. 5(a) and Fig. 6(a). At $t = t_2$, the load is added back to bus 3. The microgrid driven by OPF exhibits negative damping leading to an oscillatory instability, while SCOPF provides stable operation with a positive damping.

VI. Conclusion

This paper addresses the stable and optimal operation of inverter-populated AC microgrid. SCOPF provides the optimal operating set-points to the inverters and exhibits improved damping characteristics as compared to the operation provided by the conventional OPF. The stability constraints for the SCOPF is formulated as a bilinear-matrix inequality (BMI) constraint derived from a Lyapunov stability candidate. The SCOPF formulation is non-convex due to the presence of multiple non-linear terms. To make it computationally efficient, we have relaxed this problem using two distinct convex relaxation techniques, namely, SDP and parabolic relaxations. Further, to guarantee a globally optimal solution for SCOPF, the sequential penalization method is adopted. To prove solution scalability, several numerical studies were carried out on multiple standard IEEE and European test systems. Further, the feasibility and the efficacy of the proposed SCOPF is evaluated on a 4-inverter microgrid system emulated in a HIL setup.

References

[1] G. Agundis-Tinajero, N. L. D. Aldana, A. C. Luna, J. Segundo-Ramírez, N. Visairo-Cruz, J. M. Guerrero, and J. C. Vazquez, "Extended-optimal-power-flow-based hierarchical control for islanded ac microgrids," *IEEE Transactions on Power Electronics*, vol. 34, pp. 840–848, Jan 2019.

[2] N. Pogaku, M. Prodanovic, and T. C. Green, "Modeling, analysis and testing of autonomous operation of an inverter-based microgrid," *IEEE Transactions on Power Electronics*, vol. 22, pp. 613–625, March 2007.

[3] R. Majumder, "Some aspects of stability in microgrids," *IEEE Transactions on Power Systems*, vol. 28, no. 3, pp. 3243–3252, Aug 2013.

[4] R. Majumder, B. Chaudhuri, A. Ghosh, R. Majumder, G. Ledwich, and F. Zare, "Improvement of stability and load sharing in an autonomous

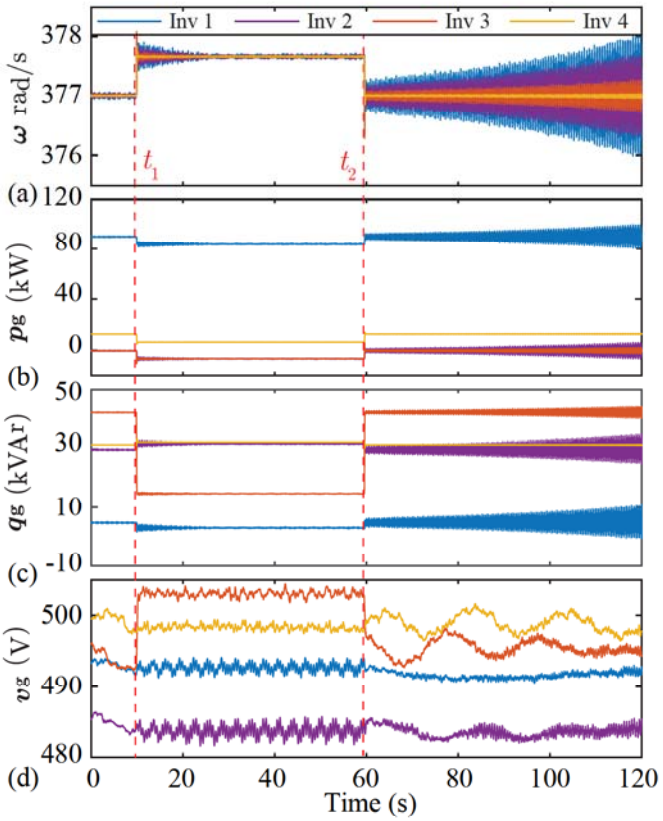

Fig. 5: Microgrid performance with optimal set-points provided by conventional OPF with the load at bus 3 disconnected and reconnected at $t = t_1$ and $t = t_2$: (a) frequency, (b) active power, (c) reactive power, and (d) voltage magnitude.

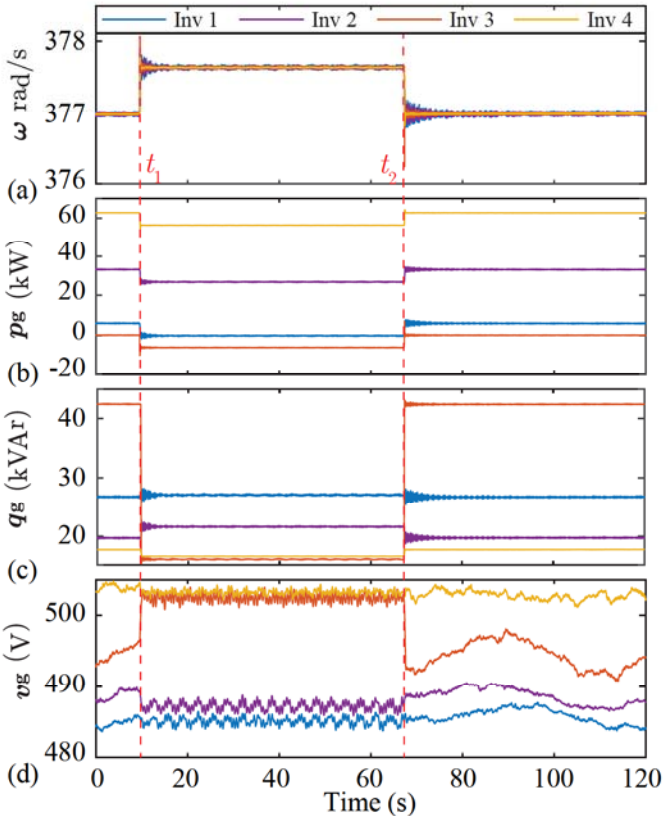

Fig. 6: Microgrid performance with optimal set-points provided by SCOPF with the load at bus 3 disconnected and reconnected at $t = t_1$ and $t = t_2$: (a) frequency, (b) active power, (c) reactive power, and (d) voltage magnitude.

microgrid using supplementary droop control loop," *IEEE Transactions on Power Systems*, vol. 25, no. 2, pp. 796–808, May 2010.

[5] A. Kahrobaeian and Y. A. I. Mohamed, "Analysis and mitigation of low-frequency instabilities in autonomous medium-voltage converter-based microgrids with dynamic loads," *IEEE Transactions on Industrial Electronics*, vol. 61, no. 4, pp. 1643–1658, April 2014.

[6] A. Firdaus and S. Mishra, "Mitigation of power and frequency instability to improve load sharing among distributed inverters in microgrid systems," *IEEE Systems Journal*, pp. 1–10, 2019.

[7] A. Trivedi and M. Singh, "l_1 adaptive droop control for ac microgrid with small mesh network," *IEEE Transactions on Industrial Electronics*, vol. 65, no. 6, pp. 4781–4789, June 2018.

[8] X. Guo, Z. Lu, B. Wang, X. Sun, L. Wang, and J. M. Guerrero, "Dynamic phasors-based modeling and stability analysis of droop-controlled inverters for microgrid applications," *IEEE Transactions on Smart Grid*, vol. 5, no. 6, pp. 2980–2987, Nov 2014.

[9] D. K. Dheer, V. A. S, O. V. Kulkarni, and S. Doolla, "Improvement of stability margin of droop-based islanded microgrids by cascading of lead compensators," *IEEE Transactions on Industry Applications*, vol. 55, no. 3, pp. 3241–3251, May 2019.

[10] J. Condren and T. W. Gedra, "Expected-security-cost optimal power flow with small-signal stability constraints," *IEEE Transactions on Power Systems*, vol. 21, no. 4, pp. 1736–1743, Nov 2006.

[11] R. Zarate-Minano, F. Milano, and A. J. Conejo, "An opf methodology to ensure small-signal stability," *IEEE Transactions on Power Systems*, vol. 26, no. 3, pp. 1050–1061, Aug 2011.

[12] P. Li, H. Wei, B. Li, and Y. Yang, "Eigenvalue-optimisation-based optimal power flow with small-signal stability constraints," *IET Generation, Transmission Distribution*, vol. 7, no. 5, pp. 440–450, May 2013.

[13] P. Li, J. Qi, J. Wang, H. Wei, X. Bai, and F. Qiu, "An sqp method combined with gradient sampling for small-signal stability constrained opf," *IEEE Transactions on Power Systems*, vol. 32, no. 3, pp. 2372–2381, May 2017.

[14] Y. Li, G. Geng, Q. Jiang, W. Li, and X. Shi, "A sequential approach for small signal stability enhancement with optimizing generation cost," *IEEE Transactions on Power Systems*, vol. 34, no. 6, pp. 4828–4836, Nov 2019.

[15] P. Pareek and H. D. Nguyen, "Small-signal stability constrained optimal power flow: A convexification approach," 2019. [Online]. Available: https://arxiv.org/abs/1911.12001

[16] L. Luo and S. V. Dhople, "Spatiotemporal model reduction of inverter-based islanded microgrids," *IEEE Transactions on Energy Conversion*, vol. 29, no. 4, pp. 823–832, Dec 2014.

[17] I. U. Nutkani, P. C. Loh, P. Wang, and F. Blaabjerg, "Decentralized economic dispatch scheme with online power reserve for microgrids," *IEEE Transactions on Smart Grid*, vol. 8, no. 1, pp. 139–148, Jan 2017.

[18] S. Boyd, L. E. Ghaoui, E. Feron, and V. Balakrishnan, *Linear Matrix Inequalities in System and Control Theory*. Philadelphia, PA: Society for Industrial and Applied Mathematics, 1994.

[19] F. Mei and B. Pal, "Modal analysis of grid-connected doubly fed induction generators," *IEEE Transactions on Energy Conversion*, vol. 22, no. 3, pp. 728–736, Sep. 2007.

[20] F. Zohrizadeh, M. Kheirandishfard, E. Q. Jnr, and R. Madani, "Penalized parabolic relaxation for optimal power flow problem," in *2018 IEEE Conference on Decision and Control (CDC)*, Dec 2018, pp. 1616–1623.

[21] M. Kheirandishfard, F. Zohrizadeh, and R. Madani, "Convex relaxation of bilinear matrix inequalities part i: Theoretical results," in *2018 IEEE Conference on Decision and Control (CDC)*, Dec 2018, pp. 67–74.

[22] M. Kheirandishfard, F. Zohrizadeh, M. Adil, and R. Madani, "Convex relaxation of bilinear matrix inequalities part ii: Applications to optimal control synthesis," in *2018 IEEE Conference on Decision and Control (CDC)*, Dec 2018, pp. 75–82.

[23] A. Bidram, A. Davoudi, F. L. Lewis, and J. M. Guerrero, "Distributed cooperative secondary control of microgrids using feedback linearization," *IEEE Transactions on Power Systems*, vol. 28, no. 3, pp. 3462–3470, Aug 2013.